Bulletin of the Seismological Society of America, Vol. 87, No. 1, pp. 67–84, February 1997

Modeling Finite-Fault Radiation from the ω^n Spectrum

by Igor A. Beresnev and Gail M. Atkinson

Abstract The high-frequency seismic field near the epicenter of a large earthquake is modeled by subdividing the fault plane into subelements and summing their contributions at the observation point. Each element is treated as a point source with an ω^2 spectral shape, where ω is the angular frequency. Ground-motion contributions from the subsources are calculated using a stochastic model. Attenuation is based on simple geometric spreading in a whole space, coupled with regional anelastic attenuation (Q operator).

The form of the ω^n spectrum with natural n follows from point shear-dislocation theory with an appropriately chosen slip time function. The seismic moment and corner frequency are the two parameters defining the point-source spectrum and must be linked to the subfault size to make the method complete. Two coefficients, $\Delta\sigma$ and K, provide this link. Assigning a moment to a subfault of specified size introduces the stress parameter, $\Delta\sigma$. The relationship between corner frequency (dislocation growth rate) and fault size is established through the coefficient K, which is inherently nonunique. These two parameters control the number of subsources and the amplitudes of high-frequency radiation, respectively. Derivation of the model from shear-dislocation theory reveals the unavoidable uncertainty in assigning ω^n spectrum to faults with finite size. This uncertainty can only be reduced through empirical validation.

The method is verified by simulating data recorded on rock sites near epicenters of the M8.0 1985 Michoacan (Mexico), the M8.0 1985 Valparaíso (Chile), and the M5.8 1988 Saguenay (Québec) earthquakes. Each of these events is among the largest for which strong-motion records are available, in their respective tectonic environments. The simulations for the first two earthquakes are compared to the more detailed modeling of Somerville *et al.* (1991), which employs an empirical source function and represents the effects of crustal structure using the theoretical impulse response. Both methods predict the observations accurately on average. The precision of the methods is also approximately equal; the predicted acceleration amplitudes in our model are generally within 15% of observations. An unexpected result of this study is that a single value of a parameter K provides a good fit to the data at high frequencies for all three earthquakes, despite their different tectonic environments. This suggests a simplicity in the modeling of source processes that was unanticipated.

Introduction

For the past decade, one of the most useful tools in the study of observed ground motions has been the stochastic point source model (Hanks and McGuire, 1981; Boore, 1983; Boore and Atkinson, 1987; Toro and McGuire, 1987; Ou and Herrmann, 1990; Boore *et al.*, 1992; EPRI, 1993; Atkinson and Boore, 1995; Silva and Darragh, 1995). The model has its origins in the work of Hanks and McGuire (1981), who showed that observed high-frequency (~1 to 10 Hz) ground motions can be characterized as finite-duration bandlimited Gaussian noise, with an underlying amplitude spectrum as specified by a simple seismological model of source and propagation processes. In California, a Brune (1970, 1971) point-source model, with a stress parameter of 50 to 100 bars (1 bar = 10^5 N/m^2), appears to explain the salient features of the empirical strong-motion database (Hanks and McGuire, 1981; Boore, 1983, 1986; Boore *et al.*, 1992).

In spite of this overall success, it is also well known that the point-source model breaks down in some cases, particularly near the source of large earthquakes. The effects of a large finite source, including rupture propagation, directivity, and source-receiver geometry, can profoundly influence

the amplitudes, frequency content, and duration of ground motion. A common approach to modeling these effects (Hartzell, 1978; Irikura, 1983) is to subdivide the fault into smaller parts, each of which is then treated as a point source. The ground motions at an observation point are obtained by summing the contributions over all subfaults. The basic assumptions in the implementation of this approach concern the manner in which the point sources and the effects of propagation path are defined. Finite-fault radiation models, as proposed by different investigators, differ chiefly in these assumptions.

The idea of modeling large events with a summation of smaller ones started with Hartzell (1978), who summed empirical records of foreshocks and aftershocks, with appropriate time delays, to approximate the mainshock record. In this approach, the problem of choosing the source and path models is resolved in a natural way, as they are included in the records of the small earthquakes. This methodology was tested in a number of articles (e.g., Kanamori, 1979; Irikura, 1983; Heaton and Hartzell, 1989). It has the advantage of simplicity, but its potential is limited by the fact that suitable empirical records are not always available.

A number of semi-empirical and theoretical approaches have been proposed to overcome this limitation. In these approaches, a theoretical model of source and/or path replaces empirical records. Table 1 illustrates the variations on the finite-fault theme. Somerville *et al.* (1991) and Cohee *et al.* (1991) use an observed near-field record to represent the source processes. Hartzell and Heaton (1983), Youngs *et al.* (1988), Hartzell and Langer (1993), and Haddon (1992, 1995) prescribe a source time function theoretically. Zeng *et al.* (1994) and Yu *et al.* (1995) opt for a theoretical stochastic ω^2 source spectrum. All of them use ray synthetics to theoretically simulate the propagation path, under the assumption that crustal structure is sufficiently well known.

Another approach models propagation effects empirically by using observed dependence of ground-motion amplitudes and duration on distance. A theoretical ω^2 spectrum is usually taken for the subsources. This approach cannot synthesize the total wave field but can be successfully applied to simulating shear waves, which are of the most engineering importance. A technique of this kind was applied to the simulation of data from the 1989 Loma Prieta (California) earthquake by Chin and Aki (1991) and Schneider *et al.* (1993) and has been applied to other regions by Silva *et al.* (1990) and Silva and Darragh (1995).

All of the above methods make simplifying assumptions about source and path processes. There has been no systematic evaluation of the relative performance of these methods, but none appears to offer a unique advantage of accuracy (correctness on average) or precision (capability of predicting details), relative to the others. In general, we favor using the simplest satisfactory method. This motivates us to investigate the capabilities of the stochastic model, as extended to the finite-fault case. We compare the simulations to data and to the predictions of an alternative technique that incorporates source processes and crustal structure more rigorously.

It should be noted that the stochastic method has been originally developed for simulating acceleration time histories, generally above 1 Hz, whose random features are difficult to model by the more deterministic approaches. The method is thus specifically aimed at engineering applications for intermediate- to high-frequency structures. At low fre-

Table 1
Finite-Fault Radiation Models

		How Is Source Modeled?			How is Path Modeled?	
Reference	Summation of Records of Small Earthquakes	Near-Field Empirical Record	Theoretical Source Time Function	ω^2 Spectrum	Synthetic Impulse Response	Empirical Attenuation and Duration Model
Hartzell (1978)	•					
Kanamori (1979)	•					
Irikura (1983)	•					
Heaton and Hartzell (1989)	•					
Somerville *et al.* (1991)		•			•	
Cohee *et al.* (1991)		•			•	
Hartzell and Heaton (1983)			•		•	
Youngs *et al.* (1988)			•		•	
Hartzell and Langer (1993)			•		•	
Haddon (1992, 1995)			•		•	
Zeng *et al.* (1994)				•	•	
Yu *et al.* (1995)				•	•	
Silva *et al.* (1990)				•		•
Chin and Aki (1991)				•		•
Schneider *et al.* (1993)				•		•

quencies, the deterministic methods (e.g., Somerville *et al.*, 1991) are more accurate.

Ground-Motion Simulation Technique

Stochastic Method

The stochastic modeling technique, also known as the bandlimited white-noise method, was described by Boore (1983) and applied to simulating ground motion from point sources in a number of investigations (Boore and Atkinson, 1987; Toro and McGuire, 1987; Ou and Herrmann, 1990; EPRI, 1993; Atkinson and Boore, 1995). The method assumes that the Fourier amplitude spectrum of a seismic signal can be represented as a product of the spectrum $S(\omega)$, produced by the seismic source at distance R in a lossless medium, and filtering functions representing the effects of path attenuation and site response. For a receiver installed on hard rock, for which there are no substantial site effects other than the free-surface amplification, the modulus of the shear-wave acceleration spectrum can be written as

$$A(\omega) = 2\omega^2 S(\omega) P(\omega) e^{-\omega R/2Q\beta}, \tag{1}$$

where ω is the angular frequency, Q is the quality factor, and β is the shear-wave velocity. The filter $P(\omega)$ is introduced to account for the commonly observed spectral cutoff above a certain frequency ω_m, which is believed to be caused by high-frequency attenuation by the near-surface weathered layer. In this article, $P(\omega)$ is assigned the form of the fourth-order Butterworth filter

$$P(\omega) = [1 + (\omega/\omega_m)^8]^{-1/2} \tag{2}$$

(Boore, 1983, p. 1868). It can also be modeled in terms of the spectral decay parameter κ of Anderson and Hough (1984) as

$$P(f) = \exp(-\pi\kappa f), \tag{3}$$

where $f = \omega/2\pi$. The simulations in this article are not sensitive to the form of $P(\omega)$, since it mainly affects motions at frequencies larger than ~10 Hz, which are above the frequency band of interest.

$S(\omega)$ is modeled by multiplying a certain deterministic "skeleton" function by the Fourier spectrum of windowed Gaussian noise. The deterministic function sets the average spectral shape and amplitude, while the stochastic function provides a realistic random character to the simulated time series.

The choice of a "skeleton" function to represent the source spectrum is not obvious. For example, existing models disagree on the rate of roll-off of the displacement spectrum at high frequencies. Most assume a high-frequency amplitude proportional to ω^{-2} (the "omega-square" model), but other models also exist (e.g., Aki, 1967; Boore, 1986). Existing theoretical foundations that relate a point source with an ω^n spectral shape to a fault with finite dimension remain largely heuristic. It is instructive in this regard to formally derive the ω^n spectrum from simple shear-dislocation theory. We show that this theory yields the ω^n spectrum exactly for an appropriately chosen displacement function at the source. The derived equation agrees with the form derived more intuitively by Brune (1970, 1971), but reveals significant nonuniqueness in this form.

The ω^2 and ω^3 Spectra from Point Shear-Dislocation Theory

An expression for the displacement from a point shear dislocation in a homogeneous elastic space (Aki and Richards, 1980, equation 4.32), together with a definition of the seismic moment, $M(t) \equiv \mu\bar{u}(t)A$, gives the far-field shear wave in the form

$$\mathbf{u}(\mathbf{x},t) = \frac{\mathbf{R}^{\theta\gamma}}{4\pi\rho\beta^3 R}\mu A\bar{u}'(t - R/\beta), \tag{4}$$

where $\mathbf{u}(\mathbf{x}, t)$ is the displacement at spatial point $\mathbf{x}$, ρ is density, μ is shear modulus, $R^{\theta\gamma}$ is the angular radiation pattern, $\bar{u}'(t)$ is the time derivative of the average displacement across the dislocation plane, and A is the area of the dislocation.

Boundary conditions that constrain the form of the source time function $\bar{u}(t)$ are that the displacement must start from zero and approach a certain level $\bar{u}(\infty)$ over the source rise time T. Three of the infinite number of *ad hoc* time functions satisfying these conditions are

$$\bar{u}_0(t) = \bar{u}(\infty)(1 - e^{-t/\tau}), \tag{5}$$

$$\bar{u}_1(t) = \bar{u}(\infty)\left[1 - \left(1 + \frac{t}{\tau}\right)e^{-t/\tau}\right], \tag{6}$$

$$\bar{u}_2(t) = \frac{\bar{u}(\infty)}{2}\left\{2 - \left[1 + \left(1 + \frac{t}{\tau}\right)^2\right]e^{-t/\tau}\right\}, \tag{7}$$

where τ is a characteristic time parameter controlling the rate of the displacement increase. Figure 1 illustrates these functions in dimensionless form. Their derivatives, $\bar{u}_n'(t)$, can be written as

$$\bar{u}_n'(t) = \frac{\bar{u}(\infty)}{n!\tau}\left(\frac{t}{\tau}\right)^n e^{-t/\tau}, \quad n = 0, 1, 2, \tag{8}$$

where $0! = 1$. These functions, which control the far-field displacement, are plotted in Figure 2. Two pulse shapes, corresponding to $n = 1$ and 2, are compatible with reasonable physical constraints: the displacement starts from zero as the wave arrives and returns to zero after the wave passes. The displacement given by $n = 0$ is physically unrealistic in that it has a discontinuity at $t = 0$, which would mechan-

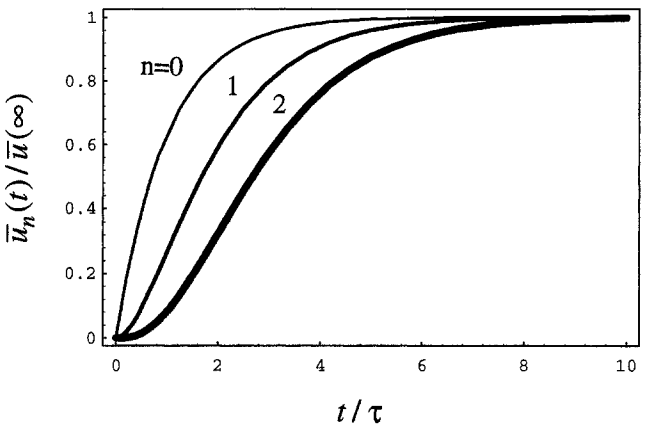

Figure 1. Theoretical source time functions (equations 5 to 7).

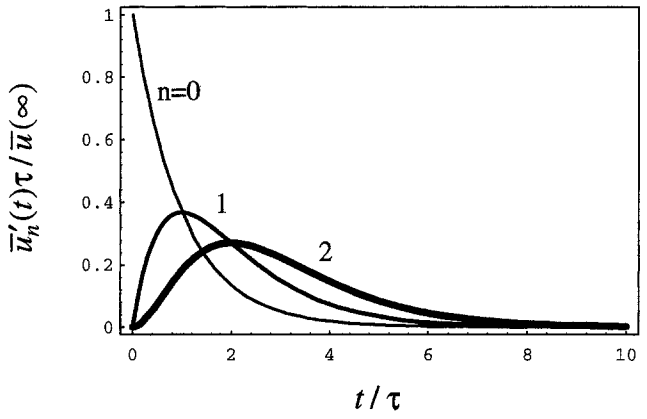

Figure 2. Theoretical shear-wave pulses in far field.

ically require an infinite stress at the tip of the rupture. Thus, the condition of smoothness of the source time function at the start and the end of slip is important. For this reason, ramp functions, such as that given by equation (5), should not be used.

Substituting equation (8) into (4), we obtain

$$\mathbf{u}_n(\mathbf{x},t) = \frac{\mathbf{R}^{\theta\varphi}M_0}{4\pi\rho\beta^3\tau R}\frac{1}{n!}\left(\frac{t - R/\beta}{\tau}\right)^n e^{-[t-(R/\beta)]/\tau}, \quad n = 1 \text{ or } 2, \quad (9)$$

where the total seismic moment released is

$$M_0 = \mu A\bar{u}(\infty). \quad (10)$$

The modulus of the Fourier transform of (9) is

$$|\mathbf{u}_n(\mathbf{x},\omega)| = \frac{\mathbf{R}^{\theta\varphi}M_0}{4\pi\rho\beta^3 R}[1 + (\omega/\omega_c)^2]^{-(n+1)/2}, \quad n = 1 \text{ or } 2, \quad (11)$$

where we have introduced the notation $\omega_c = 1/\tau$. Thus the time functions given by equations (6) and (7) yield spectra that have the same low-frequency limit but differing high-frequency behavior. The parameter ω_c is the corner frequency of the spectrum. An "omega-squared" spectrum, as developed less formally by Brune (1970, 1971), results from $n = 1$, while an "omega-cubed" spectrum results from $n = 2$. A higher-order decay is formally possible.

Equation (11) is not yet complete, for our purposes. Our goal is to apply it to simulating the radiation from a fault element with finite dimension L. Thus we must relate L to the parameters M_0 and ω_c (or τ) of an equivalent point source.

From equations (6) and (7), we can link τ to the rise time of the small source (T). Because the duration of slip in the exponential functions (6) and (7) is formally unlimited, the rise time can be defined as the time during which the average slip reaches a certain fraction x of $\bar{u}(\infty)$. A common convention is to define the rise time as corresponding to $x = 0.5$, but this choice is not unique. For $x = 0.5$, then defining $T/\tau \equiv z$, the ω^2 model (6) gives

$$(1 + z)e^{-z} = 0.5, \quad (12)$$

from which we find that $z = 1.68$ or $f_c \equiv \omega_c/2\pi = 0.27/T$. Similarly, the ω^3 model yields $z = 2.67$. Thus we can relate ω_c to the above-defined rise time of a small finite source. The other expressions often proposed are $f_c = 1/T$ (Boore, 1983, equation 6), $f_c = 0.5/T$ (Boatwright and Choy, 1992), or $f_c = 0.37/T$ (Hough and Dreger, 1995, p. 1582). There is no formal reason to favor any of these specific choices, as they are simply conventions that depend on how the duration (the value of x) is defined.

It remains to relate the subevent rise time T to the dimension L of the subfault. We assume that slip at every point on the subfault continues until the rupture reaches its periphery and stops. If the rupture velocity is $V = y\beta$, where y is a constant, then the rise time is approximately

$$T = L/2y\beta, \quad (13)$$

where the average rupture propagates half of the distance L (i.e., rupture from the middle of the fault). It is another convention to decide whether a divisor of 2 should appear in equation (13). Since $T = z/\omega_c$, the corner frequency in terms of L is

$$f_c = \frac{yz}{\pi}\frac{\beta}{L}. \quad (14)$$

Thus, equation (14) has a form of $f_c = K(\beta/L)$. For circular faults, the value of $K = 0.37$ was developed by Brune (1970, equation 36), then corrected by Brune (1971), with L being the fault radius. However, the shear-dislocation formalism applied here shows that no unique correspon-

dence exists between the corner frequency of the point source and the size of the real fault. Indeed, the value of $K = yz/\pi$ in (14) depends on two parameters y and z; z is arbitrarily defined, while y is not well known. The uncertainty in formulating equation (13) is also implicitly included in (14). Thus the coefficient of proportionality K becomes in effect a matter of convention. This introduces an intrinsic ambiguity in relating an ω^n point-source spectrum to a fault element of finite dimension. Equation (14) is commonly known as a spectral scaling law. Our conclusion from the foregoing discussion is that there is no physical reason to assert any particular scaling relationship.

In our case, adopting $y = 0.95$ gives $K = 0.51$ for the ω^2 model and $K = 0.81$ for the ω^3 model. The use of Brune's value of $K = 0.37$ for the ω^2 model would imply $y = 0.69$ if L is treated as equivalent to fault radius. Note that K depends not only on the choice of the model but also on the arbitrary constant x, which controls the value of z. Thus, even if the power n is fixed, K remains nonunique.

Brune *et al.* (1979) attribute possible variations in K to finite-fault directivity effects. Here we show that uncertainty in K begins at the point-source level and is primarily related at this level to the choice of the ω^n spectrum as a source representation.

The seismic moment of the point-source dislocation, as defined by equation (10), involves the final slip $\bar{u}(\infty)$. This is often expressed as a change in stress. The slip $\bar{u}(\infty)$ results in a deformation of $\bar{u}(\infty)/L$. From Hooke's law, this causes the stress change of

$$\Delta\sigma = \mu\bar{u}(\infty)/L. \tag{15}$$

Substituting $\bar{u}(\infty)$ from (15) into (10) yields

$$M_0 = \Delta\sigma LA \approx \Delta\sigma L^3. \tag{16}$$

Thus the seismic moment of the equivalent dislocation can be approximately related to its dimension through a coefficient of proportionality $\Delta\sigma$. If $\Delta\sigma$ can be independently specified, then equation (16) completes the determination of the source model given by equation (11).

The meaning of $\Delta\sigma$ should be interpreted with caution. The shear modulus μ during slippage may be considerably lower than that in the intact rock, with the exact value being poorly known. Consequently, the quantity $\Delta\sigma$ measured from equation (15) may have little to do with the actual stress change during an earthquake. This suggests that $\Delta\sigma$ is not a strictly physical parameter and may ultimately offer little advantage over the use of $\bar{u}(\infty)$. Experimentally inferred values of $\Delta\sigma$ appear to have about the same level of uncertainty as the displacement. This article follows the traditional approach of modeling point-source radiation through the stress parameter, although we point out that this is not strictly necessary.

K and $\Delta\sigma$ are the parameters providing equivalence between a fault with finite dimension L and a point source with moment M_0 and corner frequency ω_c. The coefficient K, which controls the high-frequency radiation, does have a physical meaning in the context of our model. In equation (14), K controls ω_c or τ. From equation (6), a small τ (or large K) implies a rapid growth of dislocation to its static level. Thus, K measures dislocation growth rate. This physically constrains the value of K, though it remains nonunique due to the arbitrariness residing in (12). This ambiguity limits the degree of determinism resulting from ω^n models.

The discussion so far applies to a general power n of the earthquake source spectrum. Although, from a formal point of view, there is no reason to give preference to a particular n, it has been shown by empirical comparisons that the ω^2 spectral form generally provides the best match to observed ground motions (Boore, 1983, 1986). In the following, we limit our discussion to the ω^2 spectrum and apply it to several specific finite-fault simulation problems, comparing the results with those of other more rigorous methods.

Implementation of the Method

Finite-Fault Model

In implementing a small-source summation procedure, we follow a traditional approach outlined by Hartzell (1978), Irikura (1983), Joyner and Boore (1986), Heaton and Hartzell (1989), and Somerville *et al.* (1991). The fault plane is discretized into equal rectangular elements, each of which is treated as a point source. The rupture spreads radially from the hypocenter with the velocity $y\beta$. An element triggers when the rupture reaches its center. The contributions from all elements are lagged and summed at the receiver. The time delay for an element is given by the time required for the rupture to reach the element, plus the time for shear-wave propagation from the element to the receiver. Whole-space geometry is assumed for wave propagation.

The choice of rupture propagation velocity can potentially influence the directivity of finite-fault radiation. However, the allowable range of variability in the parameter y is relatively small. In nearly all examples found in the literature, y falls within the range from 0.6 to 1.0, implying a change of less than a factor of 2. We confirmed that this variability has only a minor effect on directivity.

The number of subsources added in the simulation is constrained by the conservation of seismic moment. The point sources have identical moments, and there are $l \times m$ sources on the fault plane, where l and m are the number of elements along its length and width, respectively. To allow for the difference in slips between subevent and the large event and achieve the target moment, the elementary faults are allowed to trigger n_s times, where n_s is the nearest integer to the number on the right-hand side of the expression

$$n_s = M_l/lmM_e, \tag{17}$$

where M_l and M_e are the target-fault and subfault moments,

respectively. The time intervals between consecutive triggerings are calculated as

$$\Delta t = (i - 1 + \xi)T, \quad i = 1, n_s, \tag{18}$$

where T is the subfault rise time and ξ is a random number uniformly distributed between 0 and 1. Randomizing the time delays accounts for heterogeneity in the earthquake rupture process. This is the only stochastic element introduced in fault kinematics in this work.

A heterogeneous slip distribution on a target fault may also be specified. In this case, n_s for every individual subfault is taken as proportional to the integer ratio of slip on this subfault to the all-fault average slip, so that the total number of point sources required by moment conservation remains unchanged. Such a representation means that the moments of asperities can only change in integer increments of M_e, which we do not regard as a major obstacle. Discretization leaves only an integer number of equivalent sources on the fault plane and makes the simulated moment discrete as well. This is an inherent feature of all models employing summation of small events, including those that use aftershocks as empirical source functions.

There is a certain freedom in choosing the subfault size L. Ideally, this should be the size of the dominant asperities, though this information is rarely available, especially for future events. From the practical standpoint, we are interested in the gross features of faulting only; this restricts the maximum necessary number of subfaults. On the other hand, a certain minimum number is also required to (1) reproduce the finite-fault geometry and rupture-propagation effects and (2) to obtain realistic-looking accelerograms. Thus, the range of possible subfault-size change is somewhat constrained, though not entirely unambiguous. In all validation studies below, the number of subfaults is kept between approximately 40 and 80. This is a rather empirical rule; within this range, the total radiation may still be dependent on L. To quantify this dependence more rigorously, we note the following. At low frequencies (below the corner frequency of subfaults f_c), the moment conservation condition constrains the amplitudes of summed radiation. At high frequencies (above f_c), subsource spectral level (a_{hf}) is proportional to $M_0 f_c^2$ (equation 11, $n = 1$). From (14) and (16), $f_c \sim L^{-1}$ and $M_0 \sim L^3$, thus $a_{hf} \sim L$. Suppose that contributions from N subsources are summed. Due to incoherence of summation at high frequencies, the summed radiation amplitude ($a_{hf\Sigma}$) increases as $\sqrt{N} a_{hf}$ (Joyner and Boore, 1986). Because $N \sim L^{-2}$, we find that $a_{hf\Sigma} \sim L^{-1}L = 1$; thus, radiation at both low- and high-frequency ends is approximately independent of L.

The problem of evaluating the dependence of the total radiation on the subfault size L is thus reduced to a question of whether f_c lies within the frequency range of interest. We will discuss this question for each of the three validation studies given below.

One way to avoid prescription of a specific subfault size is to introduce a power-law distribution of sizes over the fault plane (Frankel, 1991; Zeng *et al.*, 1994). To date, numerical implementations of this approach (Zeng *et al.*, 1994; Yu *et al.*, 1995) have required the subfaults to overlap. This implies that some parts of the fault plane radiate energy more than once, as constituents of different subsources. This seems physically unreasonable, since the rupture process traverses the fault plane only once. Furthermore, the complications introduced by the distribution of subsource sizes do not appear to be required in order to satisfactorily model the ground motion, as will be shown in this article.

Significant effort has been made recently to establish summation rules that conserve self-similar relationships between the spectra of small events and the modeled large event (Joyner and Boore, 1986; Wennerberg, 1990; Tumarkin *et al.*, 1994). This would imply that equivalence between the size of the fault and the ω^2 spectrum, which is ambiguously defined even at the subsource level, should be extrapolated to the large faults as well. This is a questionable assumption, having no firm theoretical or empirical basis. We thus see no reason to follow the summation constraints imposed by self-similarity. In our simulations, then, only the total moment and $\Delta\sigma$ constrain the number of sources. This is similar to the approach taken by Somerville *et al.* (1991, p. 5).

Point-Source Model

The amplitude spectrum of the shear wave from an elementary source is calculated using equations (1) and (2). The right-hand side of (1) is multiplied by a factor of $1\sqrt{2}$ to project the displacement vector onto one horizontal component. The source spectrum $S(\omega)$ is defined by equation (11), with $n = 1$. A spatial average of 0.55 is assumed for the radiation pattern (Boore and Boatwright, 1984). The simulations are carried out for hard-rock sites; therefore, no site terms are included in (1). The inverse Fourier transform converts calculated spectra into acceleration time histories.

Each time series of Gaussian noise is windowed using a boxcar window with a 2% cosine taper at both ends. One realization of noise provides one subevent spectrum. No attempts are made to represent the median spectrum by doing a number of simulations for a given subevent and taking their average; we discuss this type of random variability in the results in a later section. The duration of the subfault time window (T_w) is represented as the sum of its source duration (T) and a distance-dependent term (T_d):

$$T_w = T + T_d(R). \tag{19}$$

The increase in duration with distance simulates the effects of multi-pathing and scattering in the modeling procedure, which may vary regionally. It is the distance-dependent duration that enables us to successfully model the earthquake wave field at regional distances, where complicated phases such as the *Lg* wave dominate (see The Saguenay Earthquake, below). Reasonable accuracy is achieved despite the

lack of wave-propagation effect modeling through a crustal structure. T_d may be determined from empirical analysis of the seismograms of small earthquakes (e.g., Atkinson, 1993, 1995).

The subfault spectral model requires specification of the input parameters L, $\Delta\sigma$, y, z, and the elastic constants of the medium. The source duration then follows using equation (13), the corner frequency is derived from (14), and the moment of the subfaults follows from (16). Equation (16) couples with the moment conservation condition (17) to impose a trade-off between $\Delta\sigma$ and the number of subsources summed. For a given L, a large stress parameter implies a large subsource moment M_e, which then leads to a small total number of sources under moment conservation. This means that varying $\Delta\sigma$ in the simulations has its primary effect on the number of elementary sources, not the radiation amplitudes.

Example Applications

We verify the stochastic modeling technique by simulating strong-motion accelerograms from the 1985 (9/19) Michoacan, Mexico, the 1985 (3/3) Valparaíso, Chile, and the 1988 (11/25) Saguenay, Québec, earthquakes. The results in the first two cases are compared to data and to simulations of the same records by Somerville *et al.* (1991) using a more classical approach. The Saguenay simulations are compared to data and to several previous simulations (Somerville *et al.* 1990; Boore and Atkinson, 1992; Haddon, 1992, 1995).

The Michoacan Earthquake

Model Parameters. Somerville *et al.* (1991) chose an aftershock (4/30/86) time series, recorded near the epicenter, as an empirical source function for the elements of the Michoacan mainshock fault. Convolution with the theoretical impulse response for a layered crustal model was used to generate subsource seismograms; these were summed to produce simulated records for a number of strong-motion stations. Figure 3 shows the source and station geometry for the Michoacan earthquake as well as the fault discretization model adopted by Somerville *et al.* (1991). Each element is assigned an individual slip. All stations are classified as rock sites. The authors derived their discretized slip from the original results of Mendoza and Hartzell (1989). We use the same model in our simulations.

The target fault and other modeling parameters are summarized in Table 2. The representative subfault dimension is L = 22.5 km, which is the arithmetic average of its length and width. The subfault corner frequency calculated from (14) is 0.08 Hz. For y = 0.95, the subfault rise time from (13) is T = 3.2 sec, which is somewhat larger than the value of 2 sec used by Somerville *et al.* (1991, p. 12).

The stress parameter for the Michoacan earthquake, as determined from the static slip using a relationship equivalent to (15), is 19 bars (Anderson *et al.*, 1986). Using this value in equation (16), we obtain a moment of $M_e = 2.2 \times 10^{26}$ dyne-cm (1 dyne-cm = 10^{-7} N-m) for the subsources, which nearly coincides with the moment of the aftershock of 2.0×10^{26} dyne-cm used for modeling by Somerville *et al.* (1991). The moment ratio M_l/M_e is 64.8. From the n_s values indicated by the heterogeneous slip on the target fault, we obtain a sum of 64 point sources.

The distance-dependent duration term T_d in (19) for earthquakes in the Mexican subduction zone is assumed to be similar to that determined by Atkinson (1995) from empirical analysis of the seismograms of small earthquakes in the subduction region of southwestern Canada and the northwestern United States. The anelastic attenuation model of Castro *et al.* (1990) for Mexico is used.

The cut-off frequency f_m in equation (2) is 10 Hz for the Caleta de Campos and La Union stations, 5 Hz for La

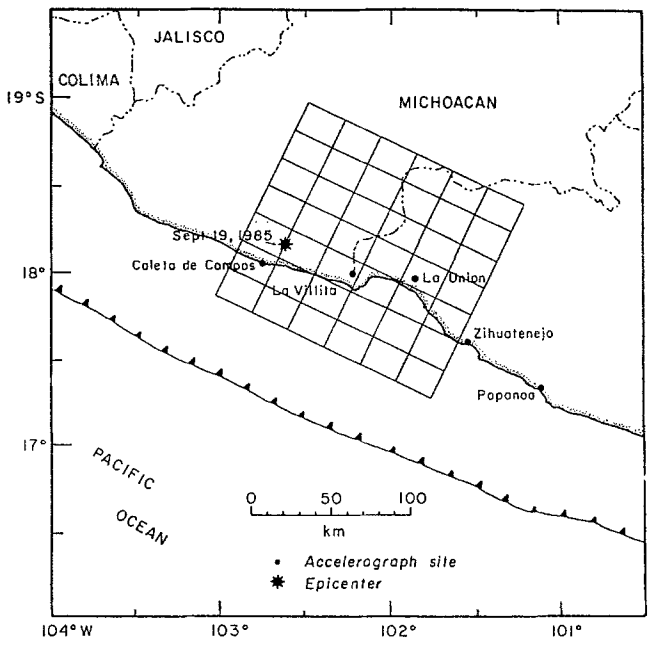

1.4	1.6	1.7	1.1	1.4	0.5
2.5	1.5	2.1	4.2	3.2	1.1
3.8	1.8	1.5	2.6	3.0	1.2
2.1	1.6	0.7	1.0	1.3	0.6
0.8	1.3	0.5	0.5	0.7	0.4
0.8	2.0	1.7	1.1	0.5	0.3
1.3	1.3	1.3	0.9	0.8	0.7

SLIP (meters)

Figure 3. Finite-fault model and epicenter of the M8.0 19 September 1985 Michoacan earthquake (after Somerville *et al.*, 1991). Results of the simulations are compared at the stations shown.

Table 2
Modeling Parameters for Mexico, Chile, and Québec Earthquakes

Parameter	Michoacan Earthquake	Chile Earthquake	Québec Earthquake
Fault orientation	Strike 300°, dip 14°	Strike 10°, dip 25°	Strike 333°, dip 51°
Fault dimensions along strike and dip (km)	150 by 140	210 by 75	14 by 2
Depth range (km)	6–40	10–40	26–27
Mainshock moment (dyne-cm)	1.4×10^{28}	1.0×10^{28}	5×10^{24}
Stress parameter (bars)	19	25	600
Subfault dimensions (km)	25 by 20	15 by 12.5	1 by 0.4
Subfault moment (dyne-cm)	2.2×10^{26}	6.5×10^{25}	2.1×10^{23}
Number of subfaults on fault plane	42	84	70
Number of subsources summed	64	156	24
Subfault rise time (s)	3.2	1.9	0.1
Subfault corner frequency (Hz)	0.08	0.14	2.6
Distance-dependent duration term (T_d) (s)	1.4 ($R \leqq 50$ km); $-2.1 + 0.07\,R$ ($R > 50$ km)	As for the Mexico earthquake	$0.16\,R$ ($R \leqq 70$ km); $-0.03\,R$ ($70 < R \leqq 130$ km); $0.04\,R$ ($R > 130$ km)
$Q(f)$	$1/(1/34 + 1/25f)$	As for the Mexico earthquake	$670f^{0.33}$
Geometric spreading	$1/R$	$1/R$	$1/R$ ($R \leqq 70$ km); $1/R^0$ ($70 < R \leqq 130$ km); $1/R^{0.5}$ ($R > 130$ km)
Windowing function	Boxcar	Boxcar	Saragoni-Hart
f_m (Hz)	5–20	10	None for six stations; 10 for stations 9, 10
Crustal shear-wave velocity (km/s)	3.7	3.8	3.65
Crustal density (g/cm^3)	2.8	2.8	2.8

Villita, 8 Hz for Zihuatenejo, and 20 Hz for the Papanoa station. These values are based on the findings of Silva and Darragh (1995). Using the κ filter (3) and the template fits to response spectral shapes for several earthquakes, they characterized these sites as having κ values of 0.045 sec (Caleta de Campos and La Union), 0.100 sec (La Villita), 0.050 sec (Zihuatenejo), and 0.020 sec (Papanoa). As seen from the relationship $f_m = 1/(\pi\kappa)$ proposed by Boore (1986, p. 58), these values are approximately equivalent to our f_m values.

Results. Figure 4 compares the observed strong-motion accelerograms for the Caleta de Campos station (nearest to epicenter; see Fig. 3) to our simulation of a random horizontal component. The corresponding simulations of Somerville *et al.* (1991) are also shown. A similar comparison is made in Figure 5 for the La Villita, La Union, Zihuatenejo, and Papanoa stations. On Figure 6, response spectra for the recorded and simulated records are compared for all the stations. Simulations for individual sites are shown for our method only since these data are not provided by Somerville *et al.* (1991). Note that the accuracy of the method is roughly independent of period over the range from 0.1 to 4 sec. Also given in Figure 6 are the arithmetic average response spectra for the five sites, as obtained from the data and the two simulation methods. A standard deviation is shown by shading around the observed average curve.

Figures 4, 5, and 6 demonstrate that the simple stochastic simulation method using the ω^2 spectra succeeds in predicting the observed amplitudes, frequency content, duration, and the overall envelope of near-field strong ground motions from the Michoacan earthquake. It compares well with the simulations of Somerville *et al.* (1991), despite the fundamental differences in assumptions and approach. This suggests that the success of the finite-fault model stems from the most basic concept of summing small earthquakes lagged in time according to the extended-fault geometry and that the details of the source and path modeling approach are less important. As seen from Figure 6, both methods closely predict the average response spectrum for rock sites; simulations are within one standard deviation of the observed average. Neither method correctly simulated the amplitudes recorded at Papanoa. This would likely be remedied by taking into account a strong site response at this station, as suggested by Somerville *et al.* (1991, p. 13). For the four sites excluding Papanoa, the method of this study predicts the individual-station peak ground accelerations (PGAs) to within 9% on average, while the alternative method is accurate to within 14%, where the error is defined as the difference between predicted and observed PGA, divided by observed PGAs.

Along with our work and the simulations by Somerville *et al.* (1991), the Caleta de Campos accelerogram during the Michoacan earthquake was also simulated by Zeng *et al.* (1994) using a power-law distribution of subevent sizes. A similar level of accuracy as that shown in Figure 4 has been achieved (see Zeng *et al.*, 1994, Fig. 4). This shows that a complication of source model, introducing a variety of subevent sizes, is not necessary to produce realistic predictions.

A limited random intraevent variability is inherent to a

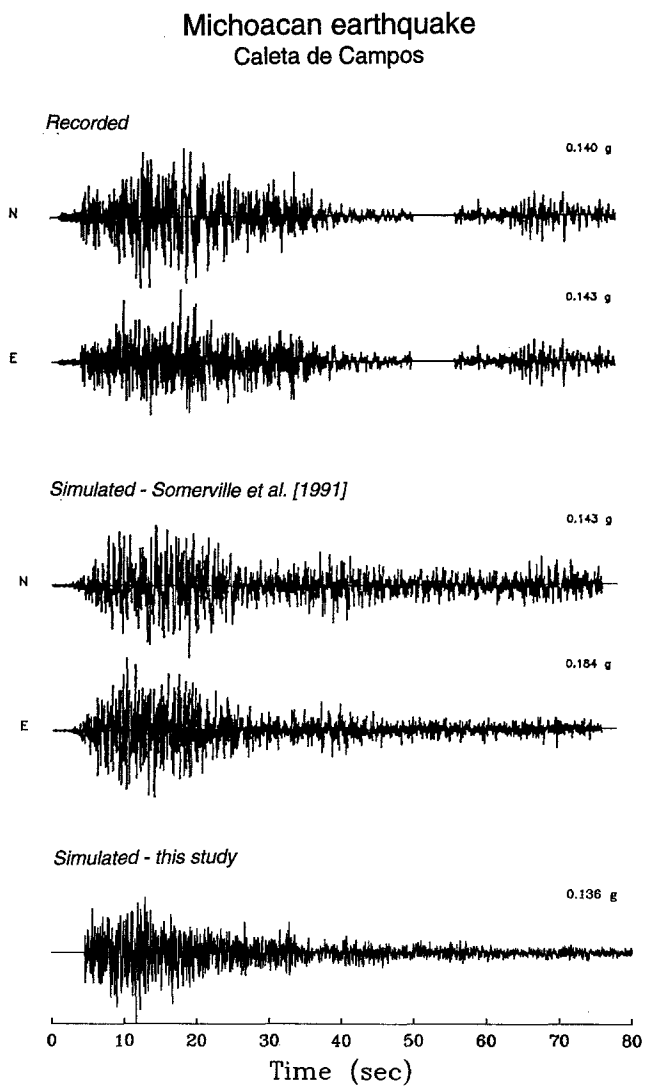

Figure 4. Comparison of horizontal acceleration time histories, recorded at Caleta de Campos station during the 1985 Michoacan earthquake, with the accelerograms simulated by the method of Somerville *et al.* (1991) and the method of this study. Peak accelerations in fractions of g are shown above accelerograms.

stochastic method of generating accelerograms. We assess the degree of this variability by simulating the ground motions for the Caleta de Campos station 10 times using different seeds of Gaussian random-number generator. The average response spectrum obtained for the 10 simulations, together with standard deviation, is plotted in Figure 7. The stochastic modeling uncertainty rises from about 6% at 0.2 sec to 33% at 4 sec. The largest uncertainty at 2 to 4 sec is comparable to that of the average observed response spectrum shown in Figure 6. The variation in PGA for the 10 random simulations is 11%. A higher precision in predicting ground-motion amplitudes using a stochastic method cannot be achieved and is not warranted given the uncertainties in the physical model parameters for future events, which greatly exceed the stochastic variability.

The Valparaíso Earthquake

Model Parameters. A heterogeneous fault model for the Valparaíso earthquake from Somerville *et al.* (1991) is shown in Figure 8. This model is adopted in our study with a modification that replaces each of the 21 fault elements with four equivalent subelements having the same slip. This modification was motivated by hiatuses in the simulated time histories that arose due to the relatively small number of subsources. Thus, our model has 84 fault elements instead of the 21 used by Somerville *et al.* In the cases of the Michoacan and Valparaíso events, the corner frequencies f_c of the subsources lie below the frequency range of interest, due to the large dimensions of the fault planes. As a result, the summed radiation is insensitive to the exact value of L, making the described modification possible (see related discussion of all three events below).

The overall model parameters are given in Table 2. The representative subfault dimension is $L = 13.75$ km. Choy and Dewey (1988, p. 1110) estimate a stress parameter of 25 bars, based on a definition equivalent to (15).

Results. Somerville *et al.* (1991) present results of their simulations for the Valparaíso UTFSM (Valu) rock site. As indicated by Silva and Darragh (1995), this site is characterized by $\kappa = 0.040$ sec, and so we set $f_m = 10$ Hz in our simulation. Figure 9 compares simulated and recorded horizontal accelerations at the Valu site, and Figure 10 compares response spectra. The overall character, duration, and amplitude of the observed ground motions agree well with our simulation and with the simulation of Somerville *et al.*

In the above simulations, we have made no attempts to adjust key model parameters to fit observations. For example, fine-tuning of the coefficient K could better the fit of our simulated average response spectrum in Figure 6 (Michoacan earthquake) or improve the agreement in Figure 10 (Valparaíso earthquake). However, we take a single value of K for both events. Furthermore, the total number of subevents is constrained by the moment-conservation condition.

The Saguenay Earthquake

Characteristics of the Earthquake. The Saguenay (Québec) earthquake of 25 November 1988 is the largest eastern North America (ENA) event for which good strong-motion records are available. Figure 11 shows the locations of the epicenter and the strong-motion stations that recorded the earthquake. All stations are on bedrock. The seismic moment of the mainshock, estimated by Somerville *et al.* (1990), is $M_l = 5 \times 10^{24}$ dyne-cm. As a continental intraplate event, the Saguenay earthquake occurred in a radically different tectonic environment as compared with the subduction zone earthquakes discussed previously, thus providing an alternative test for our model.

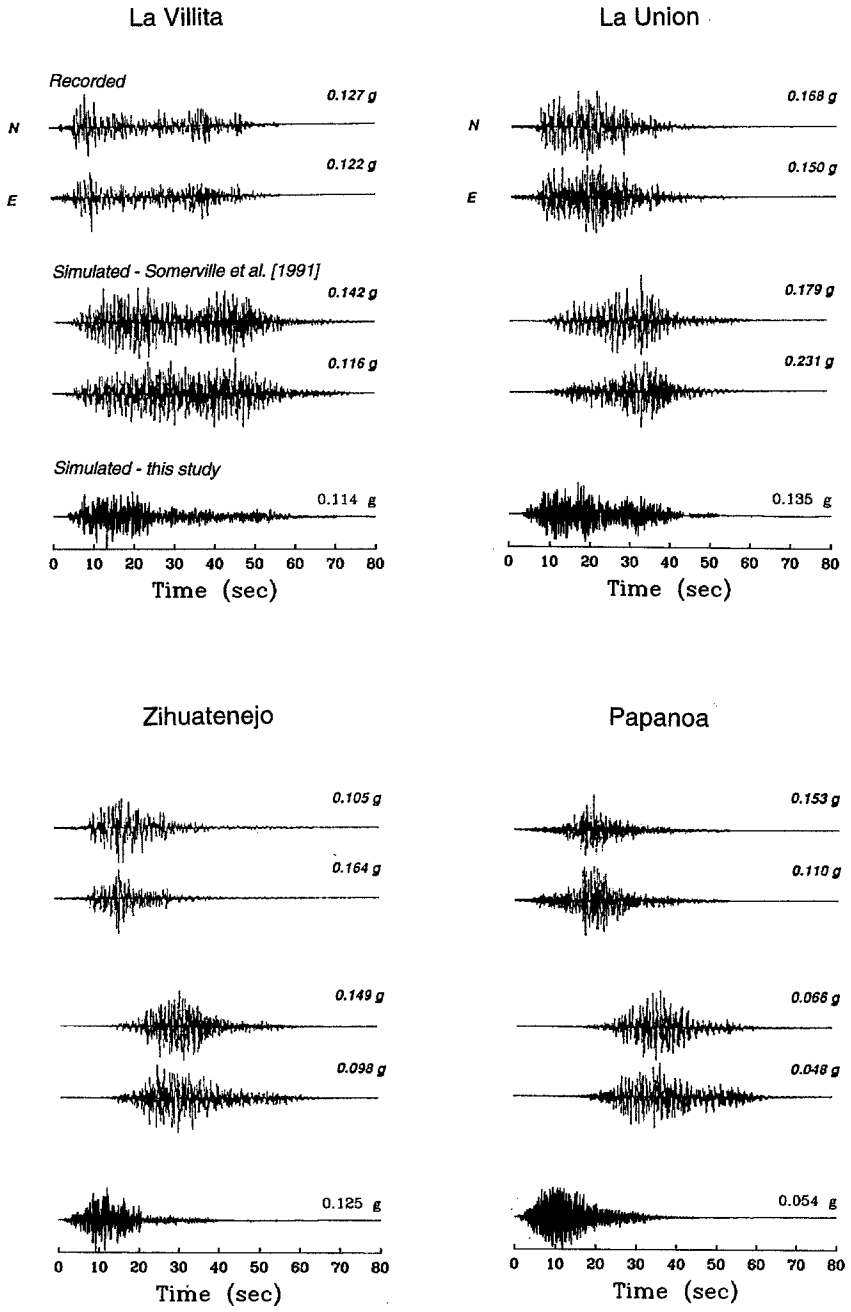

Figure 5. Observed and simulated acceleration time histories for other near-epicenter rock sites during the Michoacan earthquake. Simulations are shown for Somerville *et al.*'s (1991) method and the method adopted in this study.

The strong-motion data from the Saguenay event have been previously modeled using both a point-source approximation (Ou and Herrmann, 1990; Somerville *et al.*, 1990; Boore and Atkinson, 1992) and an extended-source geometry (Haddon, 1992; 1995; Hartzell *et al.*, 1994). The most interesting characteristic of this event is its large high-frequency energy level. Boore and Atkinson (1992) found that, for a point-source model, a stress parameter of about 500 bars was required to match these levels. Haddon (1992, 1995) found that the data might be matched by a lower stress parameter of 70 bars on average, if strong directivity effects were included. Somerville *et al.* (1990) suggested $\Delta\sigma$ of 160 bars based on teleseismic source duration but found no evidence of finite-fault effects. The wide range of stress values are not necessarily contradictory, since they are based on definitions that are not mutually consistent. No direct estimates of apparent stress change (e.g., from equation 15) are available.

Model Parameters. The longer durations of ground motion recorded at stations 16 and 17 (see Fig. 12), which are the nearest to the epicenter, indicate that fault-directivity effects in these data might be important, as suggested by Haddon (1992, 1995). The observed durations suggest the rupture propagating unilaterally toward the southeast along the northwest–southeast-extending fault. From available fault-

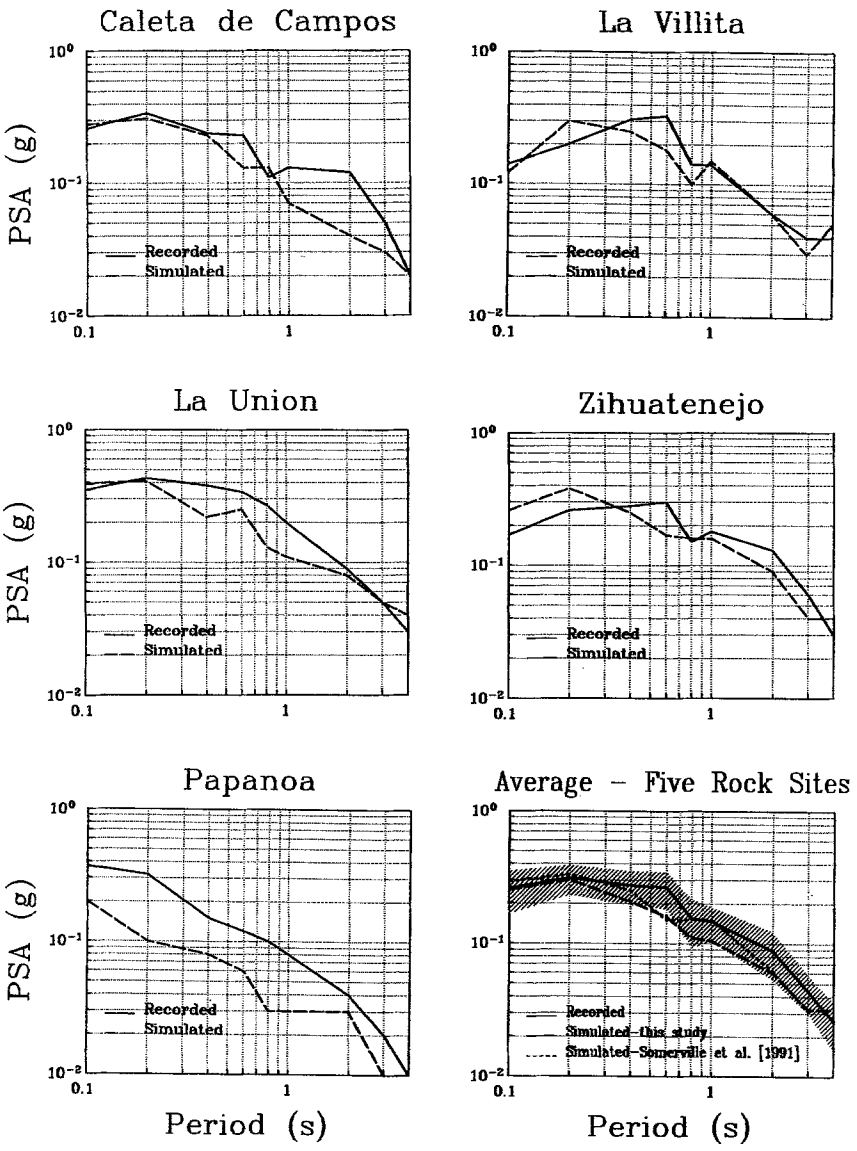

Figure 6. Comparison of the observed 5% damped pseudo-acceleration response spectra (PSA) for the rock stations Caleta de Campos, La Villita, La Union, Zihuatenejo, and Papanoa (solid lines) with the spectra simulated in this study (dashed lines). The individual observed curves are the arithmetic averages of the two horizontal components. Five-station average is also shown.

plane solutions listed in Table 2 of Haddon (1995), we adopted a fault model with strike and dip of 333° and 51°, respectively, dipping to the east. To match the duration effects in the data, we adopt fault dimensions of 14 km along strike and 2 km downdip. The fault area is thus 28 km^2. Alternative area estimates are 20 km^2 (Somerville *et al.*, 1990, p. 1126) and 15 km^2 (Haddon, 1992, p. 749).

The mainshock focal depth is in the range of 26 to 29 km (Somerville *et al.*, 1990; Boore and Atkinson, 1992; Hartzell *et al.*, 1994). We set the depth to the upper edge of the fault at 26 km. All model parameters are shown in Table 2. The fault plane is discretized into 14 elements along strike and five along dip (Fig. 11). The crack propagates unilaterally to the southeast starting at the upper northwest corner. As stated above, there is no consensus concerning the stress parameter for the Saguenay event, with values from 70 to 500 bars being reported, depending on definition. A value of 600 bars was necessary in our simulation to match the observed response spectra. We would caution against exaggerating the significance of this particular estimate though. First, a trade-off exists between $\Delta\sigma$ and the number of subsources, as discussed earlier. A restricting factor in this trade-off is the observed directivity, which requires a certain pattern of distribution of sources on the fault plane. Second, there is interplay between $\Delta\sigma$ and the duration of the modeled signal. At regional distances, the scattering and multipathing component of duration becomes very significant, as the source energy becomes drawn out over increasingly long time intervals. Models that simulate the motions based strictly on the most important ray paths (Somerville *et al.*, 1990; Haddon, 1992, 1995) will pack the energy into a shorter time window and thus require a lower stress parameter than models simulating the total duration, if the energy (moment) is conserved. An interpretation of the large implied value of $\Delta\sigma$, which follows from equation (15), is that displacement at the Saguenay source was unusually large for

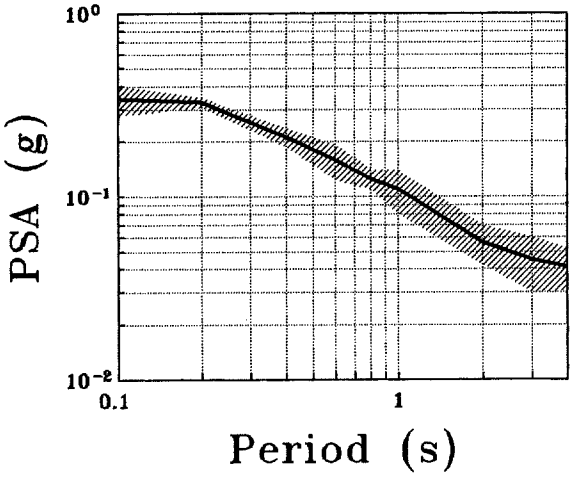

Figure 7. Average response spectrum and its standard deviation for the Caleta de Campos station, obtained from 10 stochastic simulations using different seeds of random-number generator, showing a theoretical uncertainty of the stochastic method.

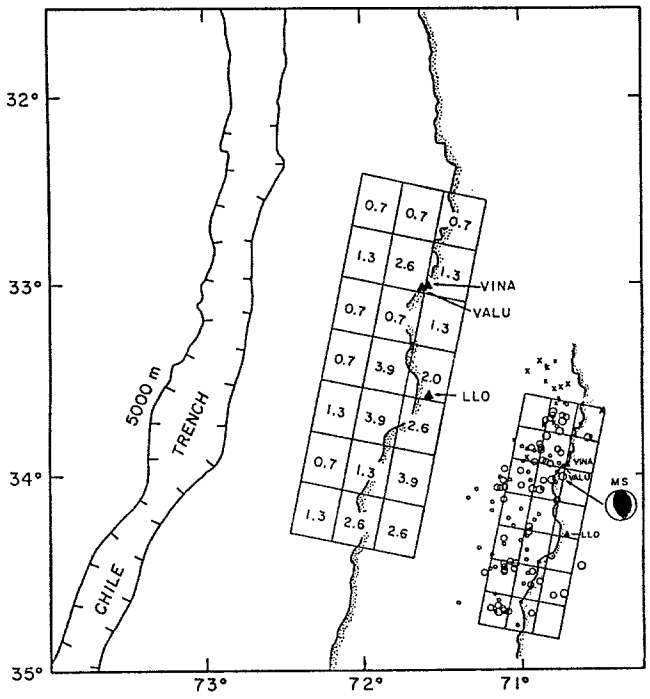

Figure 8. Fault model and epicenter of the mainshock of the 3 March 1985 M8.0 Valparaíso (Chile) earthquake, used by Somerville *et al.* (1991). Results of the two simulations are compared at the rock station Valu.

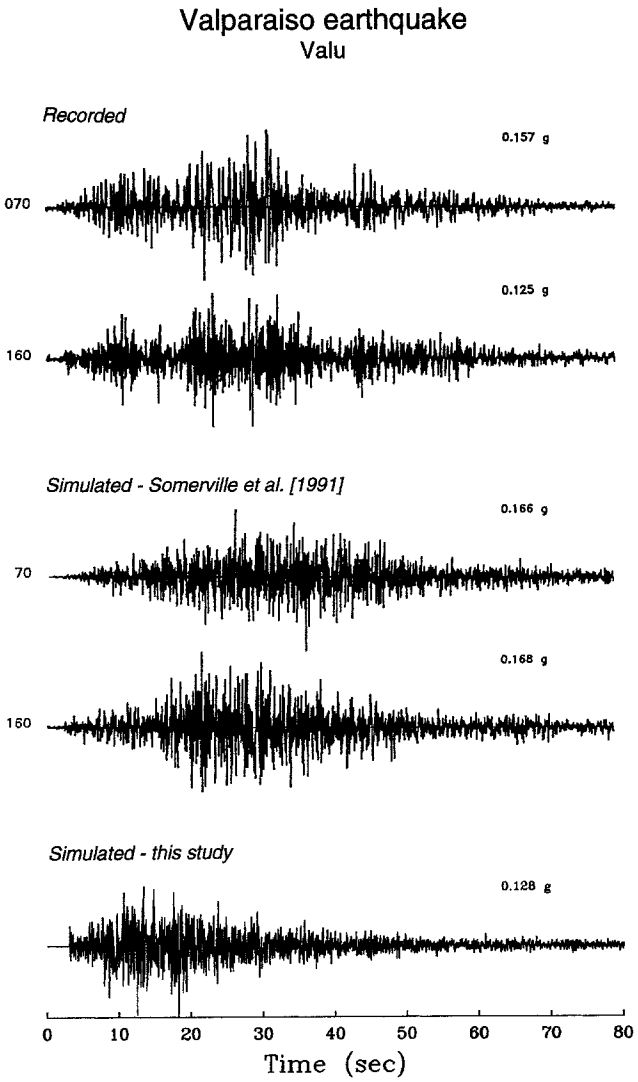

Figure 9. Horizontal acceleration time histories at Valu rock site during the 1985 Valparaíso earthquake, recorded and modeled by the two methods.

an earthquake of this size; however, this is not the only possible interpretation.

The parameter $\Delta\sigma = 600$ bars gives a ratio M_l/M_e of 24. This suggests that not all of the fault area in Figure 11, which has 70 elements, is covered by equally large slip. By best matching the data, we retained 24 subsources that are shown by hatching. These elements trigger once, and all others do not contribute to radiation. The fault model in Figure 11 is similar to that of Haddon (1992, Fig. 8), though he uses a different simulation technique. In reality, the blank elements on the fault in Figure 11 could produce a slip that was much smaller than that on the "asperities" shown by hatching. Hartzell *et al.* (1994, Fig. 15) derive an approximately 2- by 2-km dominant asperity for the Saguenay event, surrounded by a region of much-reduced slip. This result is consistent with our inference, though we used two such asperities in order to match the observed directivity.

Empirical ENA-specific duration, attenuation, and geometric spreading models were used (Atkinson and Boore, 1995, pp. 19–20). For the Saguenay earthquake, the terms T_d in (19) are comparable to the total duration T_w. In this situation, more realistic accelerogram shapes are obtained using a shaped windowing function instead of the boxcar

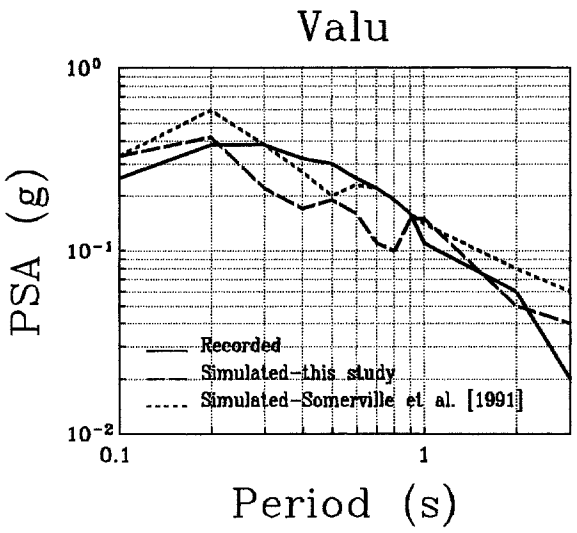

Figure 10. Observed (solid line) and simulated (dashed lines) response spectra at the Valu rock site for the Valparaíso earthquake.

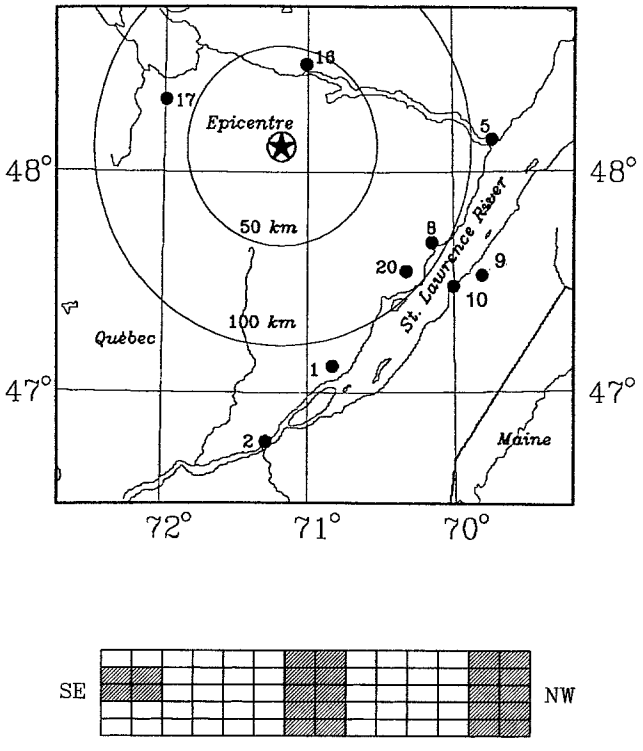

Figure 11. Locations of the epicenter of the $M5.8$ 1988 Saguenay (Québec) earthquake and stations of the Eastern Canadian Strong Motion Network that provided acceleration data (after Munro and Weichert, 1989). Bottom frame: finite-fault geometry used in the simulations. The fault is 14 by 2 km; the rupture starts at the upper element in the northwest end, and the energy is radiated by the hatched asperities.

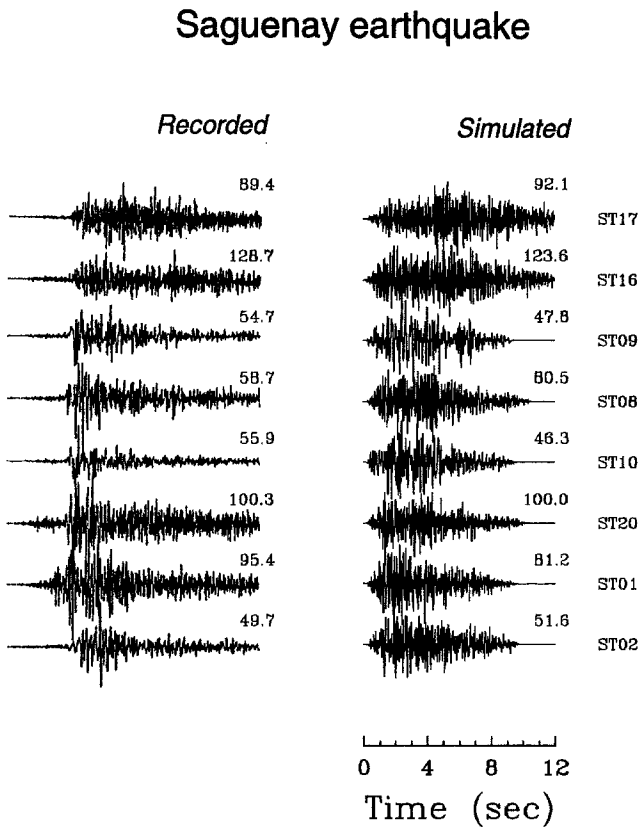

Figure 12. Recorded and simulated strong-motion accelerograms for the Saguenay earthquake. Peak acceleration in cm/s^2 is indicated above each trace; station numbers are to the right of the traces. The simulated waveforms have been scaled to the individual maximum acceleration. The recorded accelerograms have been taken from Figure 3 of Haddon (1995). In the original reference, they were multiplied by hypocentral distances measured in units of 100 km; that is, the scaling is slightly different in the left and the right panels here.

window in generating Gaussian noise samples. We adopted a Saragoni-Hart form with the parameters as defined by Atkinson and Somerville (1994, equation 2), which matches the shapes of a large number of ENA accelerograms. The crustal shear-wave velocity is from Haddon (1995, Table 1).

Unlike the rock sites in western North America, those in eastern North America show little attenuation at high frequencies (Boore and Atkinson, 1987). The cut-off frequencies f_m at all but two stations are 25 Hz, which for the frequency range of the data is equivalent to the absence of high-frequency corner. f_m at adjacent stations 9 and 10 is 10 Hz, in close agreement with observations indicating anomalous high-frequency decay at these sites (Boore and Atkinson, 1992, pp. 715–717).

Simulation of Strong-Motion Data. Figure 12 presents the observed transverse and the simulated horizontal accelerograms for the Saguenay earthquake. The simulated time

histories were high-pass filtered above a varying cut-off frequency of 0.3 to 0.8 Hz to match preprocessing of the original data (Munro and Weichert, 1989). The durations and shapes of the observed ground motion are predicted closely. The average prediction error of peak acceleration is 12%.

Observed and simulated response spectra for eight stations are compared in Figure 13. The agreement between observations and simulations is remarkably good at high frequencies (more than 2 Hz). The agreement at long periods (1 to 2 sec) is not as good, although there is some doubt concerning the reliability of the data beyond 1 sec (shown by dotting). Munro and Weichert (1989) point out that signal-to-noise ratio drops quickly in the data near the period of 2 sec, with the accelerations at longer periods being essentially noise.

Simulation of Regional Data. The above finite-fault model for the Saguenay earthquake has been derived entirely from matching strong-motion accelerograms. Apart from the strong-motion network, this earthquake was recorded by vertical instruments of the Eastern Canada Telemetered Network (ECTN). Locations of triggered ECTN stations, relative to strong-motion sites and the epicenter, are shown in Figure 14. The epicentral distances vary from 310 km (SBQ) to 472 km (GGN). By simulating ECTN data, we check if the fault model derived from strong-motion recordings is consistent with data at regional distances. To this end, we do not change the simulation procedure or the source model, except for showing the effect of incorporating an azimuthal variation in regional Q as observed by Hough *et al.* (1989).

The original ECTN velocity records have been corrected for instrument response, converted into accelerograms, and bandpass-filtered between 0.8 and 12 Hz (Boore and Atkinson, 1992). For the purpose of comparison, we convert simulated horizontal accelerations into vertical component using an empirical relationship for the Saguenay data: $H/V = 1.14 + 0.118f - 0.00638f^2$ (Boore and Atkinson, 1992, equation 3). f_m has been set to 12 Hz to match the preprocessing procedure.

Figure 15 presents recorded and simulated accelerations for the seven ECTN stations. The prominent wave packet emerging in the observed waveforms is the L_g wave. The simulations predict the characteristics of this wave train closely, despite the fact that our calculations do not model the regional crustal structure; the wave packets are simulated simply as a stochastic signal within the empirically observed distant-dependent durations. A generalized ENA duration model is used for this purpose, as obtained from hundreds of records of regional events (Atkinson and Boore, 1995). Durations are progressively dominated by the direct shear

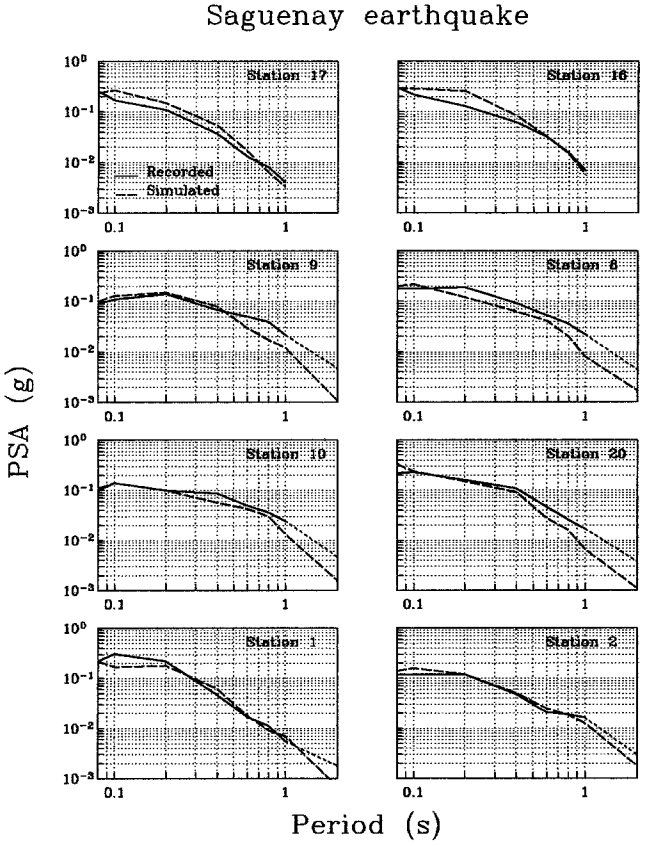

Figure 13. Observed (solid lines) and simulated (dashed lines) response spectra at strong-motion stations for the Saguenay earthquake. The observations shown are the arithmetic average of the two horizontal components. The original data are from Munro and Weichert (1989).

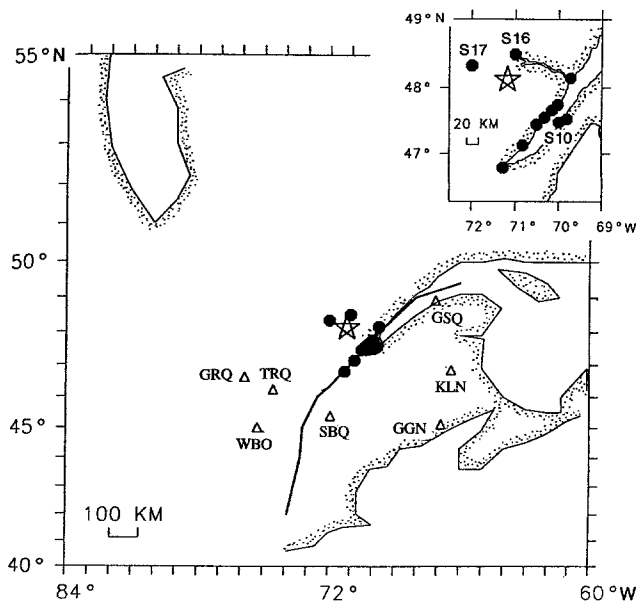

Figure 14. Regional map showing epicenter of mainshock of the Saguenay earthquake (star) and locations of the strong-motion recorders (filled circles) and ECTN stations (triangles). Strong-motion sites are the same as in Figure 11. The heavy line represents the boundary between the Grenville tectonic province (to the left) and the Appalachian tectonic province (to the right) (map after Boore and Atkinson, 1992).

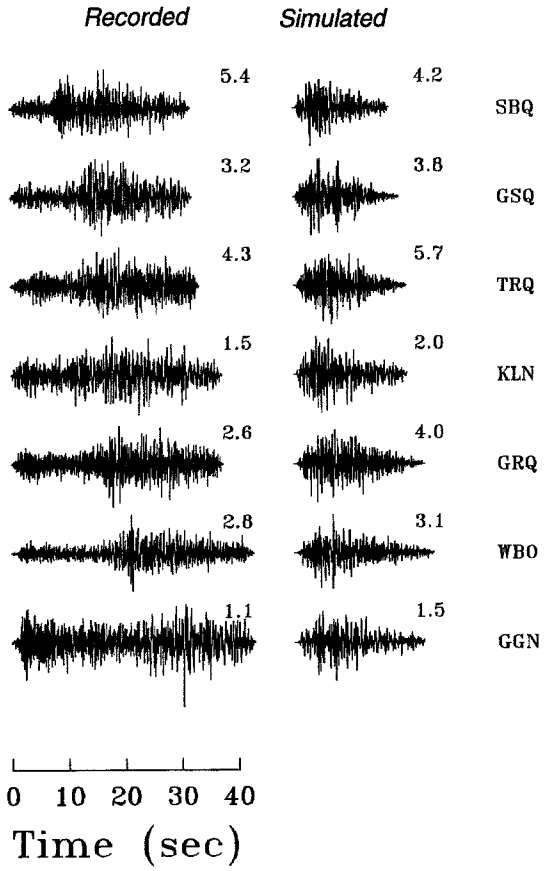

Figure 15. Recorded and simulated vertical ECTN accelerograms for the Saguenay earthquake. Simulated horizontal accelerations have been converted into vertical component using the relationship of Boore and Atkinson (1992). The waveforms are scaled to peak acceleration, which is indicated in cm/s^2 above each trace. Accelerations for stations SBQ, GSQ, KLN, and GGN have been corrected for difference in Q for paths parallel and crossing the boundary between the Grenville and Appalachian tectonic provinces (see text).

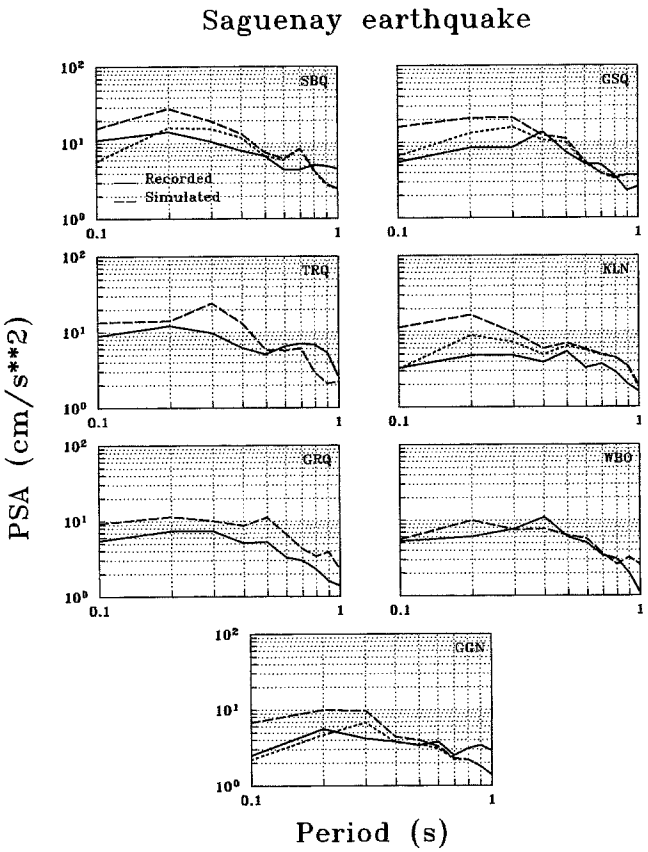

Figure 16. Observed (solid lines) and simulated (dashed lines) vertical response spectra at ECTN stations for the Saguenay earthquake. The dotted lines represent simulated spectra for four stations corrected for azimuth-dependent Q.

waves, postcritical reflected shear waves, and the L_g waves, as the signal propagates; scattering also plays an important role in duration. Our modeling results imply that this simple empirical approach is as accurate in predicting high-frequency motions as the use of more detailed crustal structure in modeling of wave-propagation effects.

In Figure 16, the recorded and simulated response spectra are presented. The low-frequency end (1 to 2.5 Hz) of the spectra is predicted satisfactorily. There is a significant overprediction of high-frequency amplitudes (3.3 to 10 Hz) at stations GSQ, KLN, and GGN. These stations are located to the south of the regional geologic boundary separating the Grenville and the Appalachian tectonic provinces, while the epicenter is to the north (Hough *et al.*, 1989, Fig. 1). Among the seven ECTN sites, the station SBQ can be attributed to the same group; its high-frequency level is also overpredicted, though to a lesser extent. The stations TRQ, GRQ, and WBO belong to the group that is to the north of the boundary; the simulation error for these three stations at high frequencies is conspicuously lower. Hough *et al.* (1989) show that the Q measured along the paths cutting across this tectonic boundary is lower than for paths parallel to it. From the frequency interval of interest in our article, Hough *et al.* (1989) estimated Q for frequencies of 1.25, 6.25, and 11.25 Hz (their Table 1). The respective ratios of Q for the paths parallel to and crossing the boundary are 1.00, 1.64, and 1.72, showing path dependence increasing with frequency. The dotted lines in Figure 16, for stations SBQ, GSQ, KLN, and GGN, represent the spectra calculated with the Q adjusted in this way. This correction nearly eliminates the apparent mismatch between observations and simulations at high frequencies. The simulated accelerograms for the same four stations, depicted in Figure 15, are those that have been adjusted for azimuthal Q variations. The average peak-acceleration prediction error is 30%.

Discussion and Conclusions

A simple summation of stochastic point sources distributed over a large fault plane is capable of simulating high-

frequency ground motions from finite faults, which are accurate on average, that is, provide near-zero average residuals. In most cases, peak acceleration amplitudes are predicted with a precision of better than 15%, although some sites may differ from predictions by factors of 2 or more, due largely to unmodeled local responses. This accuracy and precision are similar to those achieved by the more detailed modeling of Somerville *et al.* (1991). Interestingly, the method simulates near-source motions accurately despite our neglect of near-field terms in shear-dislocation radiation. This result is not fortuitous, as shown in the Appendix, and is related to the fact that we simulated only accelerations, a high-frequency measure of ground motions, and mostly above the corner frequency of the subsources. This would not be generally true for low frequencies or for displacement or velocity simulations.

Despite its apparent success, there are inherent inadequacies in the finite-fault stochastic method. Implicit in it is the assumption that a summation of small sources of size L, each characterized by an ω^2 spectrum and treated as a point source, can be used to represent the ground motion generated by the rupture on the extended fault. Strictly speaking, the only thing that justifies this assumption is that it appears to work. The transition from a small but finite rupture with dimension L to a point source with moment M_0 and corner frequency f_c is accomplished through equations (14) and (16). The concept of an equivalent point source representing each of the subfaults then enables us to simulate ground motions for wavelengths much smaller than L.

The choice of the parameter K in (14) strongly influences the simulated motions in the high-frequency range, and the accuracy of simulations hinges on this choice. It is possible to place reasonable empirical constraints on K, which ties L to dislocation growth rate, but it is ultimately nonunique. Its particular value, according to the point-dislocation model, is little more than a convention. In a sense, this nonuniqueness is the price paid for using the point-source approximation for fault elements with finite size.

The ambiguity in defining K does not necessarily limit the usefulness of the approach. Using a single adopted value of K, we successfully predict high-frequency levels of strong ground motion from three earthquakes occurring in drastically different tectonic settings, suggesting a close correspondence between the corner frequency and the size of the subfault. This finding suggests that real slip processes might be less variable than could be formally anticipated. This is an unexpected result of this modeling. It may prove, with further modeling, to be fortuitous. Thus, we cannot eliminate the likely possibility that finite-fault simulations using the stochastic technique and the ω^n spectra are inherently nonunique. Further comparative studies may show the necessity of adjusting the values of K to particular observations. The correct average K and its variability can only be established empirically.

In a hindcast simulation such as that demonstrated above, we benefit from the knowledge of an observed value of $\Delta\sigma$, as determined from fault dimensions and the final slip, except for the case of the Saguenay event. This is not the case for ground-motion forecasts. The range of possible stress-parameter values, or final fault slips, within any given region may cause significant interevent variability in ground-motion predictions. The consequence is significant uncertainty when forecasting motions from future large earthquakes, even if the location and geometry of the fault plane can be specified.

The case of the Saguenay event illustrates the effect of uncertainty in specifying the parameter $\Delta\sigma$, which, within the framework of our model, determines the number of subfaults and the "active" asperities on the fault plane. The larger is the value of $\Delta\sigma$; the lesser is the number of subevents that must be summed in order to match the required target moment. If $\Delta\sigma$ is not well known, then uncertainty in its value will lead to uncertainty in the inferred slip distribution. This may explain the differences in inferred patterns of slip across the Saguenay fault, as obtained by different authors (Haddon, 1992; 1995; Hartzell *et al.*, 1994; this article).

The choice of the representative subevent size is an issue that needs to be addressed in most finite-fault simulation methods. In our work, the fault plane is divided into approximately 40 to 80 elements. The resulting subfault corner frequencies for the Michoacan and Valparaíso earthquakes are 0.08 and 0.14 Hz, respectively (Table 2), or below the frequencies of most interest in ground-motion predictions. Finer discretization is unwarranted, since we are interested in the gross features of faulting only. Thus, all simulations for very large earthquakes (magnitudes about 8) are in the "high-frequency" domain, making the choice of subfault size L for these earthquakes unimportant. For the Saguenay event, the subfault corner frequency is 2.6 Hz, which is within the frequency range of practical interest. In this situation, the assumed subevent size should ideally correspond to the size of dominant asperities. If this information is not available, a range of L must be considered. Practically, this range can only be constrained by empirical analyses of earthquake spectra. This introduces the requirement for empirical validation of finite-fault models in each region of interest. We emphasize that the need for empirical validation with a representative range of earthquakes is common to all ground-motion prediction models.

All alternative methods presented in Table 1 have their own sources of potential bias. All finite-fault methods suffer from the necessity of making modeling assumptions that are not entirely justified. This explains the result of our particular comparison, showing that the simple stochastic technique provides a similar level of accuracy to the empirical source function method employed by Somerville *et al.* (1991). Atkinson and Somerville (1994) reached a similar conclusion comparing the two methods for small earthquakes, for which finite-fault effects could be neglected.

In conclusion, the salient features of high-frequency ground motion generated by large earthquakes can be sim-

ulated by a simple stochastic technique, which sums the contributions of equivalent point sources distributed over the rupture plane. The method has inherent ambiguity that arises from the postulated equivalence between a point source and a small but finite subsource. The ambiguous parameter K may be established on average through regional validation studies but, together with the ambiguity in specifying $\Delta\sigma$, will remain a predominant source of uncertainty in predicting the motions from future large events. This uncertainty is inherent to ground-motion prediction in general, since the detailed rupture characteristics of future earthquakes, such as the local slip rate or the value of final slip, cannot be known.

Acknowledgments

This work was supported by the Natural Sciences and Engineering Research Council of Canada. The article benefited from thoughtful reviews by M. Fehler, R. Graves, and N. Beeler.

References

Aki, K. (1967). Scaling law of seismic spectrum, *J. Geophys. Res.* **72,** 1217–1231.

Aki, K. and P. Richards (1980). *Quantitative Seismology. Theory and Methods,* W. H. Freeman and Company, San Francisco, 932 pp.

Anderson, J. and S. Hough (1984). A model for the shape of the Fourier amplitude spectrum of acceleration at high frequencies, *Bull. Seism. Soc. Am.* **74,** 1969–1993.

Anderson, J. G., P. Bodin, J. N. Brune, J. Prince, S. K. Singh, R. Quaas, and M. Onate (1986). Strong ground motion from the Michoacan, Mexico, earthquake, *Science* **233,** 1043–1049.

Atkinson, G. (1993). Notes on ground motion parameters for eastern North America: duration and *H/V* ratio, *Bull. Seism. Soc. Am.* **83,** 587–596.

Atkinson, G. M. (1995). Attenuation and source parameters of earthquakes in the Cascadia region, *Bull. Seism. Soc. Am.* **85,** 1327–1342.

Atkinson, G. M. and P. Somerville (1994). Calibration of time history simulation methods, *Bull. Seism. Soc. Am.* **84,** 400–414.

Atkinson, G. M. and D. M. Boore (1995). Ground-motion relations for eastern North America, *Bull. Seism. Soc. Am.* **85,** 17–30.

Boatwright, J. and G. Choy (1992). Acceleration source spectra anticipated for large earthquakes in Northeastern North America, *Bull. Seism. Soc. Am.* **82,** 660–682.

Boore, D. M. (1983). Stochastic simulation of high-frequency ground motions based on seismological models of the radiated spectra, *Bull. Seism. Soc. Am.* **73,** 1865–1894.

Boore, D. M. (1986). Short-period P- and S-wave radiation from large earthquakes: implications for spectral scaling relations, *Bull. Seism. Soc. Am.* **76,** 43–64.

Boore, D. M. and J. Boatwright (1984). Average body-wave radiation coefficients, *Bull. Seism. Soc. Am.* **74,** 1615–1621.

Boore, D. and G. Atkinson (1987). Stochastic prediction of ground motion and spectral response parameters at hard-rock sites in eastern North America, *Bull. Seism. Soc. Am.* **77,** 440–467.

Boore, D. M. and G. M. Atkinson (1992). Source spectra for the 1988 Saguenay, Quebec, earthquakes, *Bull. Seism. Soc. Am.* **82,** 683–719.

Boore, D., W. Joyner, and L. Wennerberg (1992). Fitting the stochastic omega-squared source model to observed response spectra in western North America: trade-offs between stress drop and kappa, *Bull. Seism. Soc. Am.* **82,** 1956–1963.

Brune, J. N. (1970). Tectonic stress and the spectra of seismic shear waves from earthquakes, *J. Geophys. Res.* **75,** 4997–5009.

Brune, J. N. (1971). Correction, *J. Geophys. Res.* **76,** 5002.

Brune, J. N., R. J. Archuleta, and S. Hartzell (1979). Far-field S-wave spectra, corner frequencies, and pulse shapes, *J. Geophys. Res.* **84,** 2262–2272.

Castro, R. R., J. G. Anderson, and S. K. Singh (1990). Site response, attenuation and source spectra of S waves along the Guerrero, Mexico, subduction zone, *Bull. Seism. Soc. Am.* **80,** 1481–1503.

Chin, B.-H. and K. Aki (1991). Simultaneous study of the source, path, and site effects on strong ground motion during the 1989 Loma Prieta earthquake: a preliminary result on pervasive nonlinear site effects, *Bull. Seism. Soc. Am.* **81,** 1859–1884.

Choy, G. L. and J. W. Dewey (1988). Rupture process of an extended earthquake sequence: teleseismic analysis of the Chilean earthquake of March 3, 1985, *J. Geophys. Res.* **93,** 1103–1118.

Cohee, B. P., P. G. Somerville, and N. A. Abrahamson (1991). Simulated ground motions for hypothesized $M_w = 8$ subduction earthquakes in Washington and Oregon, *Bull. Seism. Soc. Am.* **81,** 28–56.

EPRI (1993). Guidelines for determining design basis ground motions, Early site permit demonstration program, vol. 1, RP3302, Electric Power Research Institute, Palo Alto, California.

Frankel, A. (1991). High-frequency spectral falloff of earthquakes, fractal dimension of complex rupture, *b* value, and the scaling of strength on faults, *J. Geophys. Res.* **96,** 6291–6302.

Haddon, R. A. W. (1992). Waveform modeling of strong-motion data for the Saguenay earthquake of 25 November 1988, *Bull. Seism. Soc. Am.* **82,** 720–754.

Haddon, R. A. W. (1995). Modeling of source rupture characteristics for the Saguenay earthquake of November 1988, *Bull. Seism. Soc. Am.* **85,** 525–551.

Hanks, T. C. and R. K. McGuire (1981). The character of high frequency strong ground motion, *Bull. Seism. Soc. Am.* **71,** 2071–2095.

Hartzell, S. H. (1978). Earthquake aftershocks as Green's functions, *Geophys. Res. Lett.* **5,** 1–4.

Hartzell, S. H. and T. H. Heaton (1983). Inversion of strong ground motion and teleseismic waveform data for the fault rupture history of the 1979 Imperial Valley, California, earthquake, *Bull. Seism. Soc. Am.* **73,** 1553–1583.

Hartzell, S. H. and C. Langer (1993). Importance of model parameterization in finite fault inversions: application to the 1974 M_w 8.0 Peru earthquake, *J. Geophys. Res.* **98,** 22123–22134.

Hartzell, S. H., C. Langer, and C. Mendoza (1994). Rupture histories of eastern North American earthquakes, *Bull. Seism. Soc. Am.* **84,** 1703–1724.

Heaton, T. H. and S. H. Hartzell (1989). Estimation of strong ground motions from hypothetical earthquakes on the Cascadia subduction zone, Pacific Northwest, *Pure Appl. Geophys. (Pageoph)* **129,** 131–201.

Hough, S. E., K. H. Jacob, and P. A. Friberg (1989). The 11/25/88, M = 6 Saguenay earthquake near Chicoutimi, Quebec: evidence for anisotropic wave propagation in Northeastern North America, *Geophys. Res. Lett.* **16,** 645–648.

Hough, S. E. and D. S. Dreger (1995). Source parameters of the 23 April 1992 *M* 6.1 Joshua Tree, California, earthquake and its aftershocks: empirical Green's function analysis of GEOS and TERRAscope data, *Bull. Seism. Soc. Am.* **85,** 1576–1590.

Irikura, K. (1983). Semi-empirical estimation of strong ground motions during large earthquakes, *Bull. Disaster Prevention Res. Inst. (Kyoto Univ.)* **33,** 63–104.

Joyner, W. B. and D. M. Boore (1986). On simulating large earthquakes by Green's-function addition of smaller earthquakes, in *Proceedings of the Fifth Maurice Ewing Symposium on Earthquake Source Mechanics,* S. Das, J. Boatwright, and C. Scholz (Editors), American Geophysical Union, 269–274.

Kanamori, H. (1979). A semi-empirical approach to prediction of long-period ground motions from great earthquakes, *Bull. Seism. Soc. Am.* **69,** 1645–1670.

Mendoza, C. and S. H. Hartzell (1989). Slip distribution of the 19 September 1985 Michoacán, Mexico, earthquake: near-source and teleseismic constraints, *Bull. Seism. Soc. Am.* **79,** 655–669.

Munro, P. S. and D. Weichert (1989). The Saguenay earthquake of November 25, 1988. Processed strong motion records, *Geol. Surv. of Canada Open-File Rept. 1996,* Ottawa, Ontario.

Ou, G.-B. and R. B. Herrmann (1990). A statistical model for ground motion produced by earthquakes at local and regional distances, *Bull. Seism. Soc. Am.* **80,** 1397–1417.

Schneider, J. F., W. J. Silva, and C. Stark (1993). Ground motion model for the 1989 M 6.9 Loma Prieta earthquake including effects of source, path, and site, *Earthquake Spectra* **9,** 251–287.

Silva, W. J., R. Darragh, and I. G. Wong (1990). Engineering characterization of earthquake strong ground motions with applications to the Pacific Northwest, in *Proceedings of the Third NEHRP Workshop on Earthquake Hazards in the Puget Sound/Portland Region,* W. Hays (Editor), *U.S. Geol. Surv. Open-File Rept.*

Silva, W. J. and R. B. Darragh (1995). Engineering characterization of strong ground motion recorded at rock sites, EPRI TR-102261, Electric Power Research Institute, Palo Alto, California.

Somerville, P. G., J. P. McLaren, C. K. Saikia, and D. V. Helmberger (1990). The 25 November 1988 Saguenay, Quebec, earthquake: source parameters and the attenuation of strong ground motion, *Bull. Seism. Soc. Am.* **80,** 1118–1143.

Somerville, P., M. Sen, and B. Cohee (1991). Simulations of strong ground motions recorded during the 1985 Michoacán, Mexico and Valparaíso, Chile, earthquakes, *Bull. Seism. Soc. Am.* **81,** 1–27.

Toro, G. and R. McGuire (1987). An investigation into earthquake ground motion characteristics in eastern North America, *Bull. Seism. Soc. Am.* **77,** 468–489.

Tumarkin, A. G., R. J. Archuleta, and R. Madariaga (1994). Scaling relations for composite earthquake models, *Bull. Seism. Soc. Am.* **84,** 1279–1283.

Wennerberg, L. (1990). Stochastic summation of empirical Green's functions, *Bull. Seism. Soc. Am.* **80,** 1418–1432.

Youngs, R. R., S. M. Day, and J. L. Stevens (1988). Near field ground motions on rock for large subduction earthquakes, in *Earthquake Engineering and Soil Dynamics II—Recent Advances in Ground-Motion Evaluation,* J. Lawrence Von Thun (Editor), *Am. Soc. Civil Eng. Geotechnical Special Publication 20,* 445–462.

Yu, G., K. N. Khattri, J. G. Anderson, J. N. Brune, and Y. Zeng (1995). Strong ground motion from the Uttarkashi, Himalaya, India, earthquake: comparison of observations with synthetics using the composite source model, *Bull. Seism. Soc. Am.* **85,** 31–50.

Zeng, Y., J. G. Anderson, and G. Yu (1994). A composite source model for computing realistic strong ground motions, *Geophys. Res. Lett.* **21,** 725–728.

Department of Earth Sciences
Carleton University
1125 Colonel By Drive
Ottawa, Ontario K1S 5B6, Canada

Appendix

Validity of Far-Field Approximation for Point-Source Radiation

It has been shown above that the far-field radiation of a point-dislocation source with properly chosen slip function has an ω^n spectrum. However, a single n cannot describe both the near and far fields, and the model becomes more complicated if near-field terms are included.

The ratio of far- to intermediate- and near-field terms in equation (4.32) of Aki and Richards (1980) has an order of R/λ, where λ is the wavelength. We simulated a maximum wavelength of about 11 km (at a period of 3 sec) for the Michoacan and Valparaíso earthquakes. The minimum distance from the subsources to the recording site was within the range of 14 to 24 km for the Caleta de Campos, La Villita, La Union, and Zihuatenejo stations in the Mexico earthquake case, giving R/λ of the order of unity. This would imply that the full dislocation-radiation expression should be used instead of its truncated far-field version. In spite of this, the far-field approximation provided satisfactory results. Could it be fortuitous?

Equation (4.32) of Aki and Richards (1980) shows that intermediate- and near-field terms of the shear-dislocation radiation are time integrals of a far-field term. As a result, they have a steeper high-frequency decay beyond a common corner frequency. Acceleration spectra in the ω^2 model are dominated by frequencies higher than the corner frequency, and we simulated accelerations only. Consequently, the neglected near-field effects are relatively small even at short distances. This explains our ability to simulate the near-source motions from point sources using the far-field approximation. This would not be valid in a general case. For example, the situation would change radically if n were more than 2. For the ω^3 model ($n = 3$), simulating finite-fault radiation at close distances would necessarily require inclusion of near-field terms.

Manuscript received 12 April 1996.